

ENHANCING THERMAL PERFORMANCE AND SUSTAINABILITY Parabolic trough Concentrator Systems in Djelfa's Solar-Integrated Urban Design

by

**Salah TLILI^a, Abdelmadjid KADDOUR^b, Oumr A. OSRA^c, Mustafa BAYRAM^{d*},
Muhammad ATIF^e, Hijaz AHMAD^{f,g}, and Younes MENNI^{h,i}**

^a Development of New and Renewable Energies in Arid and Saharan Zones Laboratory (LARENZA), Department of Physics, Faculty of Mathematics and Material Sciences, Kasdi Merbah Ouargla University, Ouargla, Algeria

^b Applied Research Unit for Renewable Energies, URAER, Renewable Energy Development Center, CDER, Ghardaia, Algeria

^c Department of Islamic Architecture, Faculty of Engineering and Islamic Architecture Umm Al-Qura University, Makkah, Saudi Arabia

^d Department of Computer Engineering, Biruni University, Istanbul, Turkey

^e Department of Physics and Astronomy, College of Science, King Saud University, Riyadh, Saudi Arabia

^f Section of Mathematics, International Telematic University Uninettuno, Roma, Italy

^g Operational Research Center in Healthcare, Near East University, Nicosia, Mersin, Turkey

^h Department of Technology, University Center Salhi Ahmed Naama (Ctr. Univ. Naama), Naama, Algeria

ⁱ National University of Science and Technology, Dhi Qar, Iraq

Original scientific paper

<https://doi.org/10.2298/TSCI2304251T>

In this study, the coldest days of 2022 in the Djelfa region, Algeria, were determined using astronomical and climatic data. The timing of sunrise, sunset, and duration of sunlight, as well as changes in solar radiation intensity and air temperature, were analyzed. By converting solar radiation into heat and solving differential equations, the study examined water exit temperature, thermal energy, and total yield as outputs of a renewable energy converter. The effect of different glass coverings on these outputs was also investigated. The coldest day in 2022 was found to be the first day of January, with nine hours and 43 minutes of sunlight, a maximum solar radiation intensity of 670.34 MW/m², and a maximum air temperature of 16.9 °C. The outputs of the solar center followed a parabolic pattern for the first two parameters and increased over time for the remaining outputs, regardless of the glass type. However, using glass with a high emission coefficient, such as clear monochromatic glass, resulted in the highest values for the outputs: 52.57 °C, 7.5 kW, 162 MW, and 70.62%. By understanding solar energy conversion and thermal behavior, the study contributes to energy-efficient designs and renewable integration, aiding in sustainable urban development. Findings can inform decision-makers in optimizing material selection, promoting resilient infrastructure, and advancing sustainable practices for a low-carbon future.

Key words: *thermal performance, renewable energy, solar energy, sustainability, sustainable urban development, energy conversion*

* Corresponding author, e-mail: mbyram34@gmail.com

Introduction

The parabolic trough concentrator (PTC) is a solar concentration technology designed to convert the energy from sunlight into thermal energy. The PTC has two main applications: concentrated solar power (CSP) plants and desalination processes. In CSP plants, PTC are connected to steam power cycles, reaching temperatures of 300-400 °C. The concentration ratio is a key factor in the thermal efficiency of the collector [1]. However, desalination through reverse osmosis is energy-intensive and reliant on fossil fuels [2]. Allam *et al.* [3] shows that the helical shaft insert increases the required pumping power for the same flow rate but enhances the thermal performance of the parabolic trough collector with increased rotational speed. Mathematical models, such as the one developed by Kasem *et al.* [4], aid in design optimization using MATLAB genetic algorithm.

Research by Indira *et al.* [5] revealed that increasing the aperture width of the PTC reduces the loss in concentration caused by the compound parabolic concentrator shadow in a hybrid system. The hybrid CPC/PTC system achieves a maximum optical efficiency of ~73%, surpassing the standard PTC by ~6.35%. Manikandan *et al.* [6] found that PTC efficiency decreases as inlet fluid temperature and mass-flow rates increase due to radiation losses. Fatouh *et al.* [7] focused on designing a PTC for IPH applications in Egypt, while Wirz *et al.* [8] analyzed an alternative PTC design showing similar increases in thermal efficiency. In terms of heat transfer characteristics, Saad *et al.* [9] found that rectangular fins with round edges perform better than those with sharp edges in solar PTC.

Habchi *et al.* [10] conducted a study focusing on minimizing two significant problems: cracking of Therminol VP1 and heat loss. They aimed to mitigate these issues as much as possible. Gong *et al.* [11] introduced a novel approach by incorporating a flat reflector into the absorber tube. This modification aimed to enhance the intercept factor, optical efficiency, and overall performance of the PTC. In a separate study, Jing-Hu *et al.* [12] proposed a multi-stage heating technology to enhance efficiency and outlet temperature in PTC. Their approach involved utilizing a single-loop system consisting of a semi-circular absorber tube with two outer fins, along with a combination of semi-circular and circular absorber tubes. This innovative design enabled a significant temperature increase from 300 °C to 580 °C. Azizi *et al.* [13] conducted an analysis of a photovoltaic-thermal system that utilized a PTC with an eccentric receiver. Their study focused on evaluating the electrical, thermal, and overall efficiencies of the system. Tang *et al.* [14] proposed a novel method for designing an additional secondary reflector in PTC. The objective was to improve the distribution of heat flux on the surface of the absorber tube. By optimizing the location of the absorber, they achieved a well-balanced heat flux between the upper and lower surfaces of the tube, enhancing overall performance. In another study, Loni *et al.* [15] investigated a PTC system featuring a linear cubical cavity receiver that operated using thermal oil as the working fluid. Their research aimed to explore the characteristics and performance of this configuration.

This study investigates the use of different types of coated glass materials for a solar concentrator's heat-absorbing tube and fluid carrier. Two main sections of glass will be examined, each utilizing different types. The goal is to explore the potential benefits of this approach in cost-effective and renewable water heating. The study area chosen is a high plateau known for its cold climate year-round. The coldest day of the year will be specifically chosen to validate the proposal. To ensure the study validity, a previous study fulfilling specific criteria must be found, including astronomical location determination, accurate temperature data, and detailed information about the concentrator. The main objective is to

evaluate the thermal performance of a PTC system using Djelfa data and SAM software for analysis and assessment.

The PTC system design

The PTC under investigation is visually depicted in the accompanying diagram, providing a comprehensive illustration of its configuration and components. This visual representation offers a clear and concise overview of the studied parabolic trough concentrator, allowing for a better understanding of its structure and key elements, fig. 1.

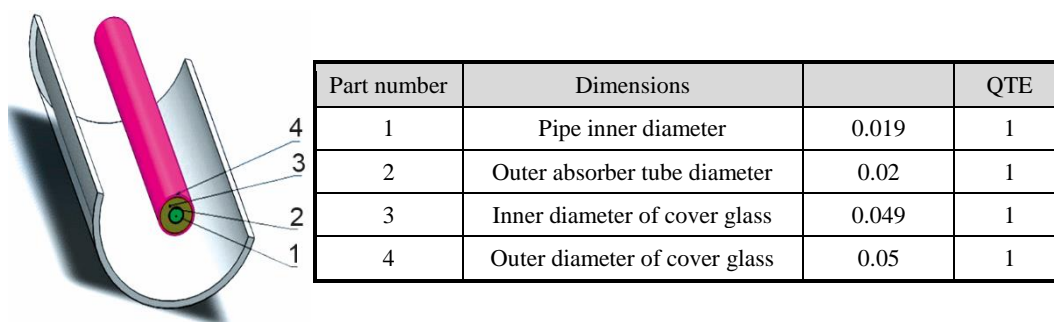


Figure 1. The design of the studied solar concentrator

In order to conduct such studies effectively, it is crucial to carefully select a specific area and time frame for analysis. Each region possesses unique characteristics determined by its astronomical location, including factors such as its elevation above sea level, latitude, and longitude. Additionally, the monthly maximum and minimum air temperatures provide vital insights into the climate of the chosen location. Depending on the research objectives, the study period can span a few hours, a complete day, or even multiple days. For this particular investigation, the Djelfa area was deliberately chosen as the study site. Situated at an altitude of 1138 m above sea level, Djelfa is geographically positioned at 34.68° longitude and 3.27° latitude. The monthly maximum temperatures, $T_{a(max)}$, and minimum temperatures, $T_{a(min)}$, for this region are recorded and presented in tab. 1, offering valuable data for analysis and comparison throughout the study.

Table 1. Monthly maximum and minimum temperatures for the Djelfa region in 2022 [16]

Month	$T_{a(max)}$ [°C]	$T_{a(min)}$ [°C]	Month	$T_{a(max)}$ [°C]	$T_{a(min)}$ [°C]
January	16.89	8.95	07	46.15	33.67
February	20.16	8.83	08	42.71	31.60
March	34.35	17.87	09	42.80	29.27
April	33.93	21.66	10	30.88	21.05
May	39.12	25.48	11	32.11	18.17
June	46.28	31.41	12	20.84	10.30

In terms of the study period, the choice in this study was the coldest day of the year, which was determined by searching for the lowest values of the highest air temperature on all days of the year, using the following relation [17, 18]:

$$T_a = \left[\frac{T_{a(\max)} - T_{a(\min)}}{2} \right] \cos \left[\frac{(14-t)\pi}{12} \right] + \left[\frac{T_{a(\max)} + T_{a(\min)}}{2} \right] \quad (1)$$

where t is the local time. To calculate T_a during the daytime period, it is necessary to restrict the calculation to the local time span between sunrise and sunset. This time range is determined concurrently with the calculation of solar radiation intensity for the corresponding day. In arid regions, the total solar radiation is equivalent to its direct component, which, after being concentrated by solar concentrators, is transformed into heat. This transformation is governed by the principles of heat exchange, which can be simulated using the electrical system depicted in fig. 2. The sky temperature, T_s , is derived using the following relationship [19]:

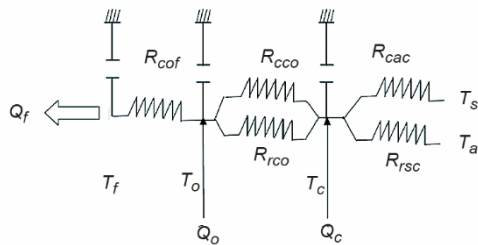


Figure 2. Electrical model representation of heat exchangers in the solar concentrator

$$T_s = 0.0552T_a^{1.5} \quad (2)$$

The presented figure demonstrates that the heat exchangers are arranged in three distinct layers. This configuration is attributed to the utilization of a linear PTC with an absorbent tube that is coated with a layer of glass.

A comprehensive explanation of this arrangement can be found in the meticulous study conducted by [20]. Consequently, the specific values of the resistors employed in the model are provided:

$$R_{cof} = \frac{1}{h_{cof}}, \quad R_{cco} = \frac{1}{h_{cco}}, \quad R_{cac} = \frac{1}{h_{cac}}, \quad R_{rco} = \frac{1}{h_{rco}}, \quad R_{rsc} = \frac{1}{h_{rsc}} \quad (3)$$

$$Q_o = wLI_d C_g \rho^0 \tau_c \alpha_o, \quad Q_c = wLI_d C_g \rho^0 \tau_c \alpha_c, \quad Q_f = \dot{m}_f C_{p,f} (T_{ff} - T_{fi}) \quad (4)$$

where C_g represents the angle of incidence modified according to [21]. As is commonly understood, these concentrators are comprised of a cylindrical reflector with a parabolic-shaped cross-section (width $w = 3$ m). Within the concentrator, a copper tube, known as the absorbent element, is securely positioned along its length ($L = 5$ m). This copper tube is hollow, allowing for the passage of fluid (water) through it. In our study, we explore the modification of the envelope glass type (single or double; clear, tinted, reflective, or low-e), as indicated by Guan [22], which directly impacts the coefficients Q_o and Q_c mentioned earlier, in addition to other variables:

$$h_{rco} = \frac{\sigma(T_o + T_c + 546.3)[(T_o + 273.15)^2 + (T_c + 273.15)^2]}{\frac{1}{\varepsilon_o} + \frac{1 - \varepsilon_c}{\varepsilon_c} \left(\frac{D_{oe}}{D_{oi}} \right)} \quad (5)$$

To simplify the analysis of the concentrator, several assumptions are made. These assumptions are based on idealizing the concentrator and creating a manageable framework. The key assumptions include assuming a uniform temperature distribution across the heat-collecting element due to the non-vacuum-sealed glass envelope. The negligible thickness of small surfaces allows their impact on the overall system to be ignored. Heat transfer is approximated as 1-D for PTC systems with a length less than 100 m, implying no significant temperature differences between different cross-sections of the heat-collecting element. The system is assumed to be thermally stable, maintaining a relatively constant temperature under normal conditions. The water flowing inside the absorbent tube is assumed to remain in a continuous liquid phase without undergoing phase changes. Additionally, perfect solar tracking ensures accurate alignment of the concentrator with the sun's position, without any tracking errors.

Results and discussions

Identifying the study day: unveiling key observations and insights

Figure 3 presents the curve derived from calculations of the highest daily air temperature values in the Djelfa region for 2022. The curve shows consistent temperature values throughout each month. Notably, the lowest temperature occurs on January 1st, the start of the year, with sunrise at 7:08 a. m. and sunset at 4:52 p. m., resulting in approximately 9 hours and 43 minutes of sunlight.

During the study day, the total radiation intensity is estimated to be 15.27 MW/m², and correspondingly, the hourly rate of radiation can be calculated as 15.27 MW/hr/m². Solar radiation becomes noticeable after approximately 47 minutes, albeit in a very weak amount, as indicated in tab. 2. This table documents the recorded values of radiation intensities at sunset, as well as the corresponding air temperatures during these specific times. It is important to note these details for anyone undertaking this research.

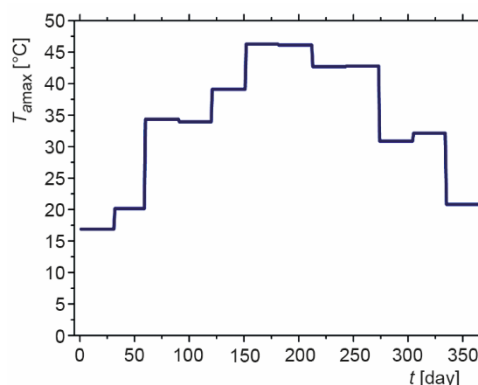


Figure 3. Daily air temperature variation throughout the year 2022 in the Djelfa region

Table 2. Timing, intensity of direct solar radiation, and air temperature at sunrise, onset of radiation, and sunset

	Sunrise	The onset of radiation	Sunset
Timing	7 hours and 8 minutes	7 hours and 55 minutes	16 hours and 52 minutes
Direct radiation intensity [Wm ⁻²]	0	5.63E-02	194.77
Air temperature [°C]	12.03	12.84	15.83

Analysis of direct solar radiation intensity on the study day

Figure 4(a) depicts a curve illustrating the changes in direct solar radiation intensity throughout the study day, following a parabolic pattern. The lowest intensity of 20.62 MW/m^2 is observed at 8:00 a. m., significantly lower by 352.27 MW/m^2 compared to the intensity recorded at 4:00 p. m.

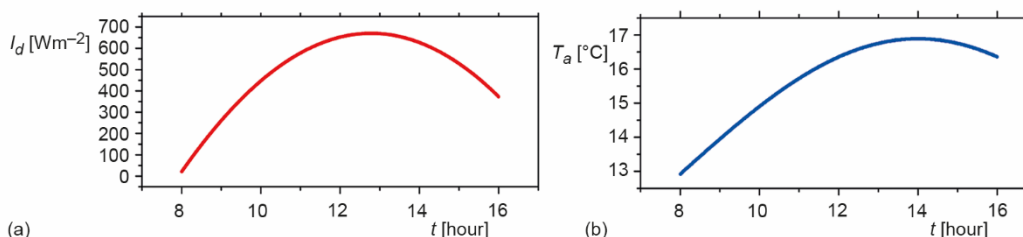


Figure 4. Temporal evolution of; (a) direct solar radiation intensity and (b) air temperature from eight in the morning until four in the evening on January 1, 2022, in the Djelfa region

Around thirteen minutes prior to one hour after noon, the highest intensity of radiation is recorded, estimated at 670.34 MW/m^2 . Over the course of the eight-hour study period, the total radiation intensity on this particular day can be estimated at 14.38 MW/m^2 , equivalent to an hourly rate of radiation of 1.8 MW/hr/m^2 .

Comprehensive analysis of air temperature patterns

The fluctuations in air temperature throughout the study day, from 8:00 a. m. to 4:00 p. m., are depicted in fig. 4(b). The maximum recorded air temperature during this period is $16.9 \text{ }^\circ\text{C}$, observed around 2:00 p. m. The temperature starts $4 \text{ }^\circ\text{C}$ lower than the peak value and gradually increases nearly linearly with a slope of $0.86 \text{ }^\circ\text{C}$ per hour until midday. After reaching the highest point, the temperature follows a nonlinear pattern, gradually declining by only $0.54 \text{ }^\circ\text{C}$ by the end of the calculation period. Overall, the variation in air temperature throughout the day resembles a parabolic shape.

Analysis of solar concentrator outputs

Analysis of water exit temperature

The temperature difference between the water leaving the solar concentrator and the surrounding air was analyzed throughout the study day within a specific area. Two curves in fig. 5 illustrate the temperature difference: curve A for single glazing and curve B for double glazing. Both curves show a parabolic pattern, resembling the trends observed in direct solar radiation and air temperature. This correlation indicates a significant impact of these factors on the temperature of the water leaving the concentrator.

Figure 5 and tab. 3 illustrate the temperature differences of water exiting the solar concentrator. Initially, the disparity between the temperatures is small, with a maximum of $1.57 \text{ }^\circ\text{C}$ for single clear glass and a minimum of $0.86 \text{ }^\circ\text{C}$ for double reflective glass. However, these temperatures are insufficient for personal use. Throughout the day, regardless of the glass type, the water temperatures remain below the desired range. The highest temperature differences occur around three to four minutes after noon, reaching $14.34 \text{ }^\circ\text{C}$ and $11.12 \text{ }^\circ\text{C}$ for single and double glazing respectively. By 4 o'clock, the temperature differences decrease to $8.31 \text{ }^\circ\text{C}$ and $6.51 \text{ }^\circ\text{C}$ respectively, due to a decrease in the emission coefficient.

Figure 5. Variation in temperature difference between solar concentrator water exit and ambient atmosphere on January 1, 2022, in the Djelfa region for; (a) single-glass types and (b) double-glazing models

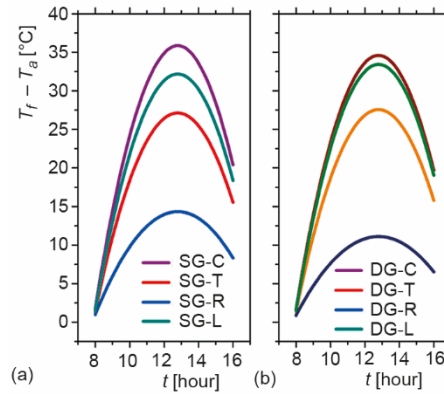


Table 3. Comprehensive analysis of PTC concentrator performance: water outlet temperatures, instantaneous and total energy, and total efficiency

Glass type		t	T_f [°C]	Q_{inst} [kW]	Q_T [MW]	R [%]
Single	Clear	8:00 h	14.49	0.33	0.06	2.65E-02
		16:00 h	36.76	4.26	161.8	70.65
		Max. value	52.57	7.50	/	/
	Tinted	8:00 h	14.23	0.28	0.05	2.33E-02
		16:00 h	31.89	3.24	122.81	53.63
		Max. value	43.84	5.67	–	–
	Reflective	8:00 h	13.87	0.20	4.00E-02	1.90E-02
		16:00 h	24.67	1.74	6.52E+01	28.48
		Max. value	31.06	2.99	–	–
	Low-e	8:00 h	14.38	0.31	0.06	2.52E-02
		16:00 h	34.73	3.84	145.5	63.53
		Max. value	48.88	6.73	–	–
Double	Clear	8:00 h	14.45	0.32	6.00E-02	2.60E-02
		16:00 h	36.04	4.11	156.09	68,16
		Max. value	51.30	7.23	–	–
	Tinted	8:00 h	14.25	0.28	5.00E-02	2.35E-02
		16:00 h	32.13	3.29	124.73	54.47
		Max. value	44.27	5.76	–	–
	Reflective	8:00 h	13.78	0.18	4.00E-02	1.78E-02
		16:00 h	22.87	1.36	508	22.18
		Max. value	27.84	2.32	–	–
	Low-e	8:00 h	14.42	0.31	6.00E-02	2.55E-02
		16:00 h	35.39	3.98	150.91	65.9
		Max. value	50.13	6.99	–	–

The maximum exit temperatures for various glass types occur around five to seven minutes before noon. Single glass types, including clear, low-e, and tinted, exhibit temperature differences compared to ambient temperature of 35.84 °C, 32.06 °C, and 27.12 °C, respectively. Double glazing temperatures for the corresponding types are 34.58 °C, 33.40 °C, and 27.54 °C. Towards the end of the computation period, the temperature differences for single and other glass types range from 15.53 °C to 20.40 °C and from 15.77 °C to 19.68 °C, respectively. The exit temperatures show a direct relationship with the emission coefficient, with higher coefficients yielding better results. In cases where emission coefficients are equal, the reflection coefficient becomes the deciding factor. While these glass types offer relatively useful exit temperatures, they still fall short of meeting personal human requirements.

Analysis of instantaneous thermal energy output

Throughout the study day, the change in thermal energy in the region displays a parabolic trend, similar to the variation in exit temperature with different glass types, fig. 6. However, a significant distinction is observed: regardless of the glass type used, the maximum value of thermal energy consistently occurs at 12 hours and 47 minutes.

These values are provided in tab. 3, which also presents the highest energy value of 7.5 kW when using single clear glass. For the remaining glass types, the energy decreases in the following order: 0.27 kW, 0.51 kW, 0.77 kW, 1.74 kW, 1.83 kW, 4.5 kW, and 5.18 kW, respectively. The table also includes the energy values at the start and end times of the calculation.

Analysis of thermal energy and total yield

Data in tab. 3 and fig. 7 indicate that the total thermal energy initially increase slowly, with closely clustered values at 8.00 hours. Within a short period, typically half an hour, the energy starts to rise significantly. This upward trend is almost linear between ten in the morning and two in the afternoon, reaching its maximum value by the end of the calculation. The total thermal energy follows the same variation pattern throughout the study day and within the region, depending on the type of glass used. The estimated total thermal energy is 161.8 MW for single pure glass, and the maximum values for other glass types range from 5.71 MW to 111 MW.

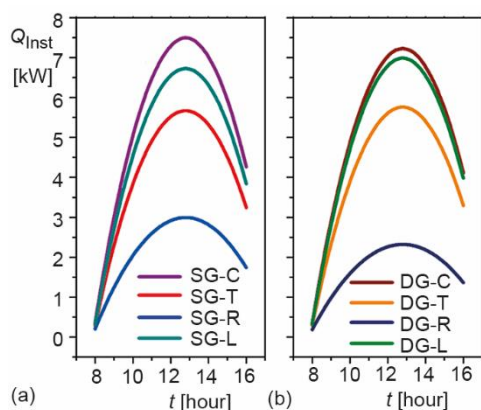


Figure 6. Variation in instantaneous thermal energy output from the solar concentrator on January 1, 2022, in the Djelfa region for; (a) single-glass types and (b) double-glazing models

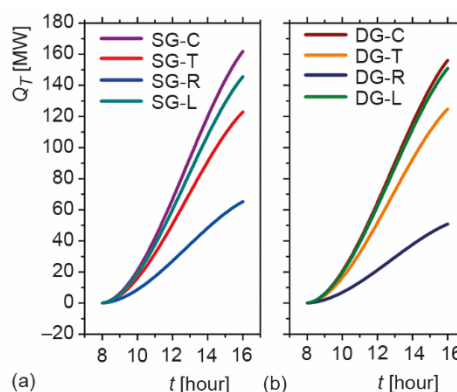


Figure 7. Variation in total thermal energy output from the solar concentrator on January 1, 2022, in the Djelfa region for; (a) single-glass types and (b) double-glazing types

Regarding the total yield, depicted in fig. 8, its change mirrors that of the total energy, despite the direct influence of radiation intensity. Table 3 further reveals that the initial value of the total yield is negligible, gradually increasing. For pure single glass, the maximum yield is estimated at 70.65%, while for the other glass types, in the usual order, the maximum values are: 2.49, 4.75, 7.12, 16.18, 17.02, 42.17, and 48.47.

Conclusions

The findings of the calculations conducted in this study have provided valuable insights. They have allowed for:

- Identification of the coldest days in the Djelfa region throughout the year 2022, specifically coinciding with the beginning of the year, *i.e.*, January 1st.
- Determination of key characteristics of this particular day, including the timing of sunrise, sunset, and the duration of sunlight. Additionally, it facilitated the observation of changes in solar radiation intensity and air temperature, both throughout the day and during the calculation period.
- Examination of the temperature variations of the water exiting the solar concentrator, which exhibited a linear parabolic pattern. This analysis encompassed the study of instantaneous and total heat energy generation, as well as the total heat yield over the course of the day. Notably, similarities were observed between the first two factors and the last two factors during a specific period of the study day.
- Establishment of an arrangement for different types of glass used as the heat-absorbing tube enclosure in the concentrator. The results indicated that better outcomes were achieved across all concentrator outputs when the glass had a higher emission coefficient. In cases where the emission coefficient was equal, emphasis was placed on a higher reflection coefficient.
- Acknowledgment of the limitations inherent in the simulation approach, which may neglect certain influential factors. This realization underscores the potential for future research, particularly in the study area.
- Incorporation of empirical measurements for solar radiation intensity, recognizing the various factors that can impact it, such as cloud cover, humidity, and the presence of airborne dust or water vapor condensation, especially during winter.

Acknowledgment

Researchers Supporting Project number (RSP2023R397), King Saud University, Riyadh, Saudi Arabia

References

- [1] Abbood, M. H., *et al.*, Design, Construction, and Testing of a Parabolic Trough Solar Concentrator System for Hot Water and Moderate Temperature Steam Generation, *Kufa Journal of Engineering*, 9 (2018) 1, pp. 42-59

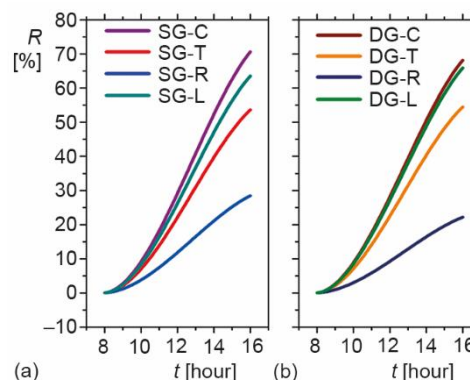


Figure 8. Variation in total heat yield from the solar concentrator on January 1, 2022, in the Djelfa region for; (a) single-glass types and (b) double-glazing models

- [2] Naveenkumar, R., et al., Comprehensive Review on Various Parameters that Influence the Performance of Parabolic Trough Collector, *Environmental Science and Pollution Research*, 28 (2021), Mar., pp. 22310-22333
- [3] Allam, M., et al., Experimental Investigation on Performance Enhancement of Parabolic Trough Concentrator with Helical Rotating Shaft Insert, *Sustainability*, 14 (2022) 22, 14667
- [4] Kasem, M. M., Multiobjective Design Optimization of Parabolic Trough Collectors, *Scientific Reports*, 12 (2022) 1, 19964
- [5] Indira, S. S., et al., Optical Performance of a Hybrid Compound Parabolic Concentrator and Parabolic Trough Concentrator System for Dual Concentration, *Sustainable Energy Technologies and Assessments*, 47 (2021), Oct., 101538
- [6] Manikandan, K. S., et al., Parametric Study of Solar Parabolic Trough Collector System, *Asian Journal of Applied Sciences*, 5 (2012), 6, pp. 384-393
- [7] Fatouh, M., et al., Performance of a Solar Thermal Parabolic Trough Concentrator for Industrial Process Heat (IPH) Applications in Egypt, in *International Solar Energy Conference*, 36762 (2003), Jan., pp. 269-278
- [8] Wirz, M., et al., Potential Improvements in the Optical and Thermal Efficiencies of Parabolic Trough Concentrators, *Solar Energy*, 107 (2014), Sept., pp. 398-414
- [9] Saad, B., et al., Thermal Enhancement of Parabolic Trough Collectors using Absorber Tubes with Internally longitudinal Round Edge Fins, *Engineering Research Journal*, 173 (2022), Mar., pp. 356-375
- [10] Habchi, A., et al., Performance Study of a New Parabolic Trough Design Under Optical Concentrator Effect, *Applied Thermal Engineering*, 219 (2023), Jan., 119500
- [11] Gong, J. H., et al., Optical, Thermal and Thermo-Mechanical Model for a Larger-Aperture Parabolic Trough Concentrator System Consisting of a Novel Flat Secondary Reflector and an Improved Absorber Tube, *Solar Energy*, 240 (2022), July, pp. 376-387
- [12] Jing-Hu, G., et al., Performance Optimization of Larger-Aperture Parabolic Trough Concentrator Solar Power Station Using Multi-Stage Heating Technology, *Energy*, 268 (2023), Apr., 126640
- [13] Azizi, M., et al., Evaluation of Mono and Hybrid Nano-Fluids on Energy and Exergy Parameters of a Photovoltaic-Thermal System Equipped with an Eccentric Parabolic Trough Concentrator, *Applied Thermal Engineering*, 223 (2023), Mar., 119979
- [14] Tang, X. Y., et al., A Design Method for Optimizing the Secondary Reflector of a Parabolic Trough Solar Concentrator to Achieve Uniform Heat Flux Distribution, *Energy*, 229 (2021), Aug., 120749
- [15] Loni, R., et al., Sensitivity Analysis of Parabolic Trough Concentrator Using Rectangular Cavity Receiver, *Applied Thermal Engineering*, 169 (2020), Mar., 114948
- [16] *** SAM software (n.d.), Retrieved May 14, 2023, from <https://sam.nrel.gov/>
- [17] Reicosky, D. C., et al., Accuracy of Hourly Air Temperatures Calculated from Daily Minima and Maxima, *Agricultural and Forest Meteorology*, 46 (1989) 3, pp. 193-209
- [18] Belghit, A., et al., Numerical Study of a Solar Dryer in Forced Convection, *Revue Generale de Thermique*, 36, (1997), 11, pp. 837-850
- [19] Garcaa-Valladares, O., Velazquez, N., Numerical Simulation of Parabolic Trough Solar Collector: Improvement Using Counter Flow Concentric Circular Heat Exchangers, *International journal of heat and mass transfer*, 52 (2009), 3-4, pp. 597-609
- [20] Fuqiang, W., et al., Progress in Concentrated Solar Power Technology with Parabolic Trough Collector system: A Comprehensive Review, *Renewable and Sustainable Energy Reviews*, 79 (2017), Nov., pp. 1314-1328
- [21] Kalogirou, S. A., Solar Thermal Collectors and Applications, *Progress in Energy and Combustion Science*, 30 (2004) 3, pp. 231-295
- [22] Guan, L., The Influence of Glass Types on the Performance of Air-Conditioned Office Buildings in Australia, *Advanced Materials Research*, 346 (2012), Sept., pp. 34-39